Re©B$_8^-$ and Re©B$_9^-$: New Members of the Transition-Metal-Centered Borometallic Molecular Wheel Family

Published as part of The Journal of Physical Chemistry virtual special issue "Hai-Lung Dai Festschrift".

Teng-Teng Chen,[†,∥] Wan-Lu Li,[‡,∥] Hui Bai,[†,⊥] Wei-Jia Chen,[†] Xin-Ran Dong,[§] Jun Li,*[,‡,§] and Lai-Sheng Wang*[,†]

†Department of Chemistry, Brown University, Providence, Rhode Island 02912, United States
‡Department of Chemistry and Key Laboratory of Organic Optoelectronics & Molecular Engineering of Ministry of Education, Tsinghua University, Beijing 100084, China
§Department of Chemistry, Southern University of Science and Technology, Shenzhen 518055, China

Ⓢ *Supporting Information*

ABSTRACT: Transition-metal-centered monocyclic boron wheel clusters (M©B$_n^q$) represent a family of interesting borometallic compounds with double aromaticity. A variety of early and late transition metal atoms have been found to form such structures with high symmetries and various B$_n$ ring sizes. Here we report a combined photoelectron spectroscopy and quantum-chemistry theoretical study of two M©B$_n^-$ clusters from the middle of the transition metal series: Re©B$_8^-$ and Re©B$_9^-$. Global minimum structure searches revealed that ReB$_8^-$ adopts a pseudo-C_{8v} structure while ReB$_9^-$ is a perfectly planar D_{9h} molecular wheel. Chemical bonding analyses showed that both clusters exhibit σ and π double aromaticity and obey the electronic design principle for metal-centered borometallic molecular wheels. The central Re atoms are found to possess unusually low oxidation states of +I in Re©B$_8^-$ and +II in Re©B$_9^-$, i.e., the Re atom behaves similarly to late transition metal elements (Ru, Fe, Co, Rh, Ir) in the M©B$_n^-$ molecular wheels. These two clusters become new members of the family of transition-metal-centered monocyclic borometallic molecular wheels, which may be viable for chemical syntheses with appropriate ligands.

ReB$_8^-$ (C_2, ^3A)   ReB$_9^-$ (D_{9h}, $^2A_1'$)
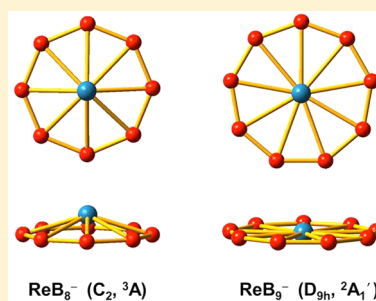
1. INTRODUCTION

Because of its electron deficiency, boron displays a large number of allotropes with complex crystal structures consisting of different polyhedral cage building blocks,[1,2] which is totally different from its neighbor carbon, which has four electron and four valence orbitals. Nanoclusters of boron have also been found to exhibit a great variety of unusual structures and chemical bonds.[3−6] Joint experimental and theoretical studies of size-selected boron clusters have led to the discoveries of tubular nanostructures,[7,8] all-boron graphene-like monolayers (borophenes),[9,10] and all-boron fullerene-like cage structures (borospherenes).[11,12] Boron also forms a class of rich metal boride materials with broad potential applications, ranging from the superconducting compound MgB$_2$ and superhard metal borides to borides with interesting magnetic properties and ultrahigh thermal conductivities.[13−16] Studies of metal boride clusters have become a new direction of research on boron clusters,[6,17−20] leading to the discoveries of metal-centered monocyclic wheels,[21] half-sandwich structures,[22,23] metalloborophene-like planar structures,[24,25] drumlike metal-doped nanotubular structures,[25−28] and inverse sandwich complexes.[29−31]

Among the metal boride clusters, the metal-centered monocyclic wheels, denoted as M©B$_n^q$, represent a family of fascinating planar aromatic borometallic systems.[21] The

Co©B$_8^-$ and Ru©B$_9^-$ clusters were the first members of this family of single-metal-doped boron clusters,[32] where the "©" symbol was initially proposed to designate a metal atom in the center of a boron ring in two dimensions. Subsequently, a variety of M©B$_n^q$-type borometallic clusters have been studied and characterized by photoelectron spectroscopy (PES) and ab initio calculations,[33,38] including Fe©B$_8^-$, Fe©B$_9^-$, Rh©B$_9^-$, and Ir©B$_9^-$. The Ta©B$_{10}^-$ and Nb©B$_{10}^-$ complexes represent the highest coordination number in the two-dimensional (2D) geometry.[37,39] An electronic design principle based on σ and π double aromaticity was advanced to explain the stability of such structures,[21,36,38] M$^{(x)}$©B$_n^{k-}$, where x is the valence of the central transition metal atom, n is the number of boron atoms in the monocyclic ring, and k is the charge of the cluster. The design principle requires that the bonding electrons in the system, the total number of which is $3n + x + k$, participate in n two-center two-electron (2c−2e) B−B peripheral σ bonds and two sets of aromatic delocalized bonds (σ and π double aromaticity according to the $4N + 2$ Hückel rule; 12 electrons for six σ and six π electrons or 16 electrons for 10 σ and six π electrons), that is, $3n + x + k = 2n + 12$ or $2n + 16$, which can

be simplified as $n + x + k = 12$ or 16. For late transition metals, the $n + x + k = 12$ electronic design principle is obeyed,[32−34] while for early transition metals, all five d orbitals were found to participate in the delocalized bonding, and the $n + x + k = 16$ electronic design principle holds.[35] Meanwhile, geometric factors of the central transition metal atom, such as the atomic radius (or orbital radial distribution), have also been found to play an important role in the formation of planar wheel-like structures.[36−38] To date, only early group VB (V, Nb, Ta) and late group VIIIB (Fe, Ru, Os, Co, Rh, Ir) transition metal elements have been investigated experimentally for their viability to form $M©B_n^{k-}$ molecular wheels with $n = 8−10$. Numerous theoretical studies have also been devoted to this class of interesting aromatic systems.[40−47] A question arises: how about the transition metal elements in the middle of the transition series? Do they form $M©B_n^{k-}$-type molecular wheels? Which electronic design principle do they obey? What is the size range of such aromatic borometallic wheels that they may form?

In the current article, we report the experimental observation and characterization of two $M©B_n^{k-}$ clusters involving Re from group VIIB, i.e., ReB_8^- and $Re©B_9^-$, using a joint PES and quantum-chemical study. Global-minimum searches showed that ReB_8^- has a triplet ground state with a pseudo-C_{8v} structure (^3A in the C_2 point group), whereas ReB_9^- has a doublet ground state with perfect D_{9h} symmetry ($^2A_1'$). Electronic structure and bonding analyses revealed that the $Re©B_n^-$ systems behave similarly to the late transition metals. It was found that because of the large atomic radius of Re, the B_8 ring is too small to fit the Re atom, resulting in out-of-plane distortion and symmetry breaking. Further chemical bonding analyses found that Re adopts the +I oxidation state in the C_2 $Re©B_8^-$ cluster and the +II oxidation state in D_{9h} $Re©B_9^-$. The latter cluster consists of three delocalized σ bonds and three delocalized π bonds, obeying the $n + x + k = 12$ electronic design principle. The current study suggests that all transition metal elements should be able to form $M©B_n^q$ borometallic molecular wheel structures.

2. EXPERIMENTAL AND THEORETICAL METHODS

2.1. Photoelectron Spectroscopy. The experiments were carried out with a magnetic-bottle PES apparatus equipped with a laser vaporization cluster source, details of which can be found elsewhere.[5,48] Briefly, the ReB_8^- and ReB_9^- clusters were produced by laser vaporization of a hot-pressed disk target made from a mixed powder consisting of Re and isotopically enriched ^{10}B. The laser-induced plasma was cooled by a high-pressure He carrier gas seeded with 5% Ar to initiate nucleation. The nascent clusters of different charge states were entrained in the carrier gas and underwent a supersonic expansion. After passing a skimmer, negatively charged clusters were extracted perpendicularly from the collimated beam and analyzed by a time-of-flight mass spectrometer. The ReB_8^- and ReB_9^- clusters of interest were selected using a mass gate and decelerated before being photodetached by the 193 nm (6.424 eV) radiation from an ArF excimer laser. Photoelectrons were collected at almost 100% efficiency by the magnetic bottle and analyzed in a 3.5 m long electron flight tube. The electron kinetic energy spectra were calibrated using the known spectrum of Bi^-, and the presented electron binding energy spectra were obtained by subtracting the kinetic energies from the photon energy used. The resolution of the apparatus was around 2.5%, that is, ~25 meV for 1 eV electrons.

2.2. Theoretical Methods. Unbiased structural searches for the global minima of ReB_8^- and ReB_9^- with different spin multiplicities were carried out using the TGMin 2.0 package.[49−51] The Perdew−Burke−Ernzerhof (PBE) generalized gradient approximation (GGA) density functional[52] and the triple-ζ Slater-type plus one polarization function (TZP) basis sets[53] were used, as implemented in the ADF 2017.114 software.[54] The relativistic effects were taken into account using the scalar relativistic zeroth-order regular approximation (ZORA),[55] whereas the spin−orbit coupling effect was not specifically evaluated. The frozen-core approximation was applied to the $[1s^2]$ core of B and the $[1s^2−4d^{10}]$ core of Re. The remaining electrons were explicitly treated variationally in the SCF procedure. In total, more than 200 structures were generated by the TGMin code for each system. Low-energy isomers within 50 kcal/mol of the global minima were further reoptimized using the hybrid PBE0/TZP method.[56] Vibrational frequency calculations were done to verify that the isomers were true minima.

The photoelectron spectra were simulated using the ΔSCF-TDDFT approach, as described in our previous work.[57] That is, the vertical detachment energies (VDEs) of the global minima were calculated by time-dependent density functional theory (TDDFT) using TZP basis sets along with the SAOP model,[58] whereas the first VDE (VDE_1) was computed as the difference in energy between the ground electronic state of the anion and that of the neutral at the anion geometry. The VDE_1 was further evaluated more accurately at the DLPNO−CCSD(T) level[59,60] utilizing the AutoAux generation procedure[61] with the Def2-TZVP basis sets[62] and the corresponding pseudopotential for Re (Def2-TZVPP).[63] We also examined the VDE_1 using the Stuttgart pseudopotential and the aug-cc-pVTZ-PP basis set for Re[64] and the cc-pVTZ basis set for B[65] to determine the effect of the basis sets on the theoretical results. The final electronic states were determined on the basis of the TDDFT calculations and group theory. Chemical bonding analyses were performed using molecular orbital (MO) theory and the adaptive natural density partitioning (AdNDP) method.[66] We also carried out linear transit (LT) calculations by constraining the geometries at each LT coordinate along the out-of-plane pathway of Re relative to the plane of the B_n rings using the PBE/TZP method for both $Re©B_8^-$ and $Re©B_9^-$ to examine how the Re and B_n ring interactions are affected by the ring size.

3. EXPERIMENTAL RESULTS

The experimental spectra of ReB_8^- and ReB_9^- at 193 nm (6.424 eV) are shown in Figure 1. The PES bands are labeled with letters (X, A, B, ...), and the VDEs measured from the maxima of all of the observed bands are given in Tables 1 and 2 for ReB_8^- and ReB_9^-, respectively, where they are compared with the theoretical results.

3.1. ReB_8^-. The 193 nm spectrum of ReB_8^- shows six resolved bands, labeled as X, A, B, C, D, and E in Figure 1a. The lowest-binding-energy band, X, gives rise to the first VDE at 3.67 eV. The first adiabatic detachment energy (ADE) is estimated from its onset as 3.40 eV, which also represents the electron affinity (EA) of the corresponding neutral ReB_8. Band A at a VDE of 3.97 eV closely follows band X. A relatively weak band B is observed at 4.41 eV, followed by an energy gap and an intense band C at 5.28 eV, beyond which the spectrum becomes quite congested. Two more bands, D at ~5.8 eV and E at ~6.2 eV, are tentatively labeled for the sake of discussion.
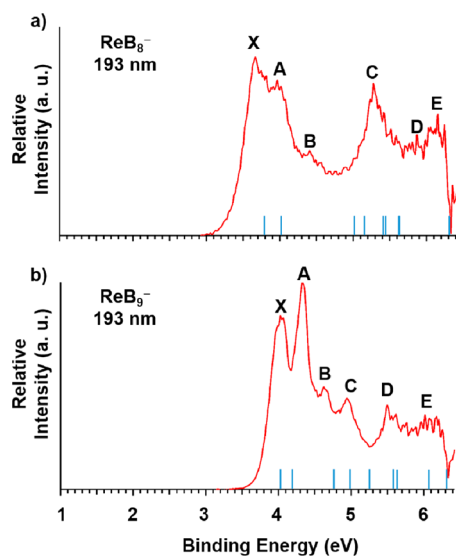
Figure 1. Photoelectron spectra of (a) ReB_8^- and (b) ReB_9^- at 193 nm (6.424 eV) and the theoretical VDEs of the global minima (represented by vertical bars).

3.2. ReB_9^-. The spectrum of ReB_9^- exhibits four well-resolved detachment transitions at the lower-binding-energy side, labeled as X, A, B, and C, as shown in Figure 1b. The intense band X yields the first VDE at 4.02 eV, while the first ADE is estimated from its onset as 3.82 eV, which also represents the EA of the corresponding ReB_9 neutral. Following band X, a sharp and more intense band A is observed at 4.34 eV. Closely following band A, two relatively weak bands are observed, B at 4.63 eV and C at 4.94 eV. Following an energy gap, a broad band D is observed at around 5.5 eV, beyond which the spectrum is not well resolved and a band E at around 6.1 eV is tentatively labeled for the convenience of discussion.

4. THEORETICAL RESULTS

4.1. Global Minima of ReB_8^- and ReB_9^-. The optimized structures within 50 kcal/mol of the global minima of ReB_8^- and ReB_9^- are presented in Figures S1 and S2, respectively. The global minimum of ReB_8^-, as shown in Figure 2, has a triplet ground state with a C_2 $Re©B_8^-$ structure, in which the Re atom is slightly out of plane relative to the B_8 ring. The distortion from C_{8v} symmetry is due to a second-order Jahn−

Teller effect. The triplet C_{8v} structure is a saddle point with imaginary vibrational frequencies and lies about 25 kcal/mol above the C_2 structure. A $Re(\eta^8\text{-}B_8)$ half-sandwich structure with C_s symmetry (3 in Figure S1) was found to lie 26 kcal/mol higher than the global minimum at the PBE0 level. The neutral $Re©B_8$ cluster has a quartet ground state with very little geometry change (Figure 2), corresponding to removal of an electron from the 14a MO, which is mainly of nonbonding Re $5d_{z^2}$ character, as shown in Figure 3.

The global minimum of ReB_9^- was found to be perfectly planar with D_{9h} symmetry and a doublet spin state, as shown in Figure 4. The nearest low-lying isomer (2 in Figure S2) has C_1 symmetry and is 11.18 kcal/mol (at the PBE/TZP level) and 19.09 kcal/mol (at the PBE0/TZP level) above the global minimum, suggesting the high stability of the D_{9h} $Re©B_9^-$ wheel structure. The singly occupied MO (SOMO) of D_{9h} $Re©B_9^-$ is mainly the Re $5d_{z^2}$ atomic orbital, as shown in Figure 5. Surprisingly, the neutral ground state of $Re©B_9$ is not obtained from detachment of the electron in the SOMO (Table 2). Instead, it arises from removal of an electron from the degenerate 7e′ HOMO (Figure 5), resulting in a triplet spin state. The ensuing Jahn−Teller effect distorts the neutral ground state to C_{2v} symmetry ($^3A_1$), as shown in Figure 4. The Cartesian coordinates of the global minima of $Re©B_8^-$ and $Re©B_9^-$ and their corresponding neutrals are given in Table S1.

4.2. Stabilities of $Re©B_8^-$ and $Re©B_9^-$ against Out-of-Plane Distortions of the Re Atom. The out-of-plane distortion of C_2 $Re©B_8^-$ suggests that the B_8 ring is too small to fit the relatively large Re atom. To quantitatively understand the relative stabilities of the $Re©B_n^-$ molecular wheels relative to different B_n ring sizes and out-of-plane distortions, we calculated the LT energy curves (Figure 6) at the PBE/TZP level by varying the Re height relative to the B_n plane, defined by the angle θ, as shown in the inset of Figure 6. The perfect D_{8h} structure of $Re©B_8^-$ is clearly shown to be a saddle point, which is 17.4 kcal/mol above the C_2 global minimum in energy at the PBE/TZP level. The value of θ at the C_2 minimum is $\pm18°$, corresponding to a Re height of 0.64 Å relative to the B_8 ring plane. At the C_2 global minimum, the B−B bond lengths on the B_8 ring range from 1.572 to 1.607 Å, and the Re−B bond lengths range from 2.155 to 2.193 Å. The B−B bond lengths in the perfectly planar $M©B_n^q$ molecular wheels range from 1.52 to 1.56 Å from previous studies[32−35] and as shown in Figure 4 for D_{9h} $Re©B_9^-$. The B−B bond lengths in the C_2

Table 1. Experimental VDEs Compared with Theoretical VDEs of the Global Minimum of $Re©B_8^-$ (C_2, ^3A) at the TD-SAOP/TZP Level[a]

observed feature	VDE (expt.)	final state and electronic configuration	VDE (theor.)
X	3.67	(^4A) ...(11b)^2(12b)^2(10a)^2(11a)^2(12a)^2(13a)^2(**14a**)^1(13b)^1(14b)^1	3.79
A	3.97	(^2A) ...(11b)^2(12b)^2(10a)^2(11a)^2(12a)^2(13a)^2(**14a**)^1(13b)^1(14b)^1	4.02
B	4.41		
C	5.28	(^2B) ...(11b)^2(12b)^2(10a)^2(11a)^2(12a)^2(13a)^2(14a)^2(13b)^1(**14b**)^0	5.02
		(^2B) ...(11b)^2(12b)^2(10a)^2(11a)^2(12a)^2(13a)^2(14a)^2(**13b**)^0(14b)^1	5.15
D	~5.8	(^4A) ...(11b)^2(12b)^2(10a)^2(11a)^2(12a)^2(**13a**)^1(14a)^2(13b)^1(14b)^1	5.41
		(^2A) ...(11b)^2(12b)^2(10a)^2(11a)^2(12a)^2(**12a**)^1(13a)^2(14a)^2(13b)^1(14b)^1	5.43
		(^2A) ...(11b)^2(12b)^2(10a)^2(11a)^2(12a)^2(**13a**)^1(14a)^2(13b)^1(14b)^1	5.62
		(^4A) ...(11b)^2(12b)^2(10a)^2(11a)^2(12a)^2(**12a**)^1(13a)^2(14a)^2(13b)^1(14b)^1	5.63
E	~6.2	(^4A) ...(11b)^2(12b)^2(10a)^2(11a)^2(**11a**)^1(12a)^2(13a)^2(14a)^2(13b)^1(14b)^1	6.32
		(^2A) ...(11b)^2(12b)^2(10a)^2(**11a**)^1(12a)^2(13a)^2(14a)^2(13b)^1(14b)^1	6.48

[a]The VDE$_1$ value was obtained from the DLPNO−CCSD(T)/Def2-TZVPP calculations. All energies are in eV.

Table 2. Experimental VDEs Compared with Theoretical VDEs of the Global Minimum of Re©B$_9^-$ (D_{9h}, ^{2}A$_1'$) at the TD-SAOP/TZP Level^a

observed feature	VDE (expt.)	final state and electronic configuration	VDE (theor.)
X	4.02	(^{3}E′) ...(2e″)^4(5a$_1'$)^2(5e′)^4(3a$_2''$)^2(6e′)^4(**7e′**)^3(6a$_1'$)^1	4.04
A	4.34	(^{1}E′) ...(2e″)^4(5a$_1'$)^2(5e′)^4(3a$_2''$)^2(6e′)^4(**7e′**)^3(6a$_1'$)^1	4.18
B	4.63	(^{3}E′) ...(2e″)^4(5a$_1'$)^2(5e′)^4(3a$_2''$)^2(**6e′**)^3(7e′)^4(6a$_1'$)^1	4.78
C	4.94	(^{1}E′) ...(2e″)^4(5a$_1'$)^2(5e′)^4(3a$_2''$)^2(**6e′**)^3(7e′)^4(6a$_1'$)^1	4.98
		(^{1}A$_1'$) ...(2e″)^4(5a$_1'$)^2(5e′)^4(3a$_2''$)^2(6e′)^4(7e′)^4(**6a$_1'$**)^0	5.25
D	5.50	(^{3}A$_2''$) ...(2e″)^4(5a$_1'$)^2(5e′)^4(**3a$_2''$**)^1(6e′)^4(7e′)^4(6a$_1'$)^1	5.57
		(^{1}A$_2''$) ...(2e″)^4(5a$_1'$)^2(5e′)^4(**3a$_2''$**)^1(6e′)^4(7e′)^4(6a$_1'$)^1	5.62
E	~6.0	(^{3}E″) ...(**2e″**)^3(5a$_1'$)^2(5e′)^4(3a$_2''$)^2(6e′)^4(7e′)^4(6a$_1'$)^1	6.06
		(^{1}E′) ...(2e″)^4(5a$_1'$)^2(**5e′**)^3(3a$_2''$)^2(6e′)^4(7e′)^4(6a$_1'$)^1	6.32
		(^{3}A$_1'$) ...(2e″)^4(**5a$_1'$**)^1(5e′)^4(3a$_2''$)^2(6e′)^4(7e′)^4(6a$_1'$)^1	6.43

^{a}The VDE$_1$ value was obtained from the DLPNO−CCSD(T)/Def2-TZVPP calculations. All energies are in eV.

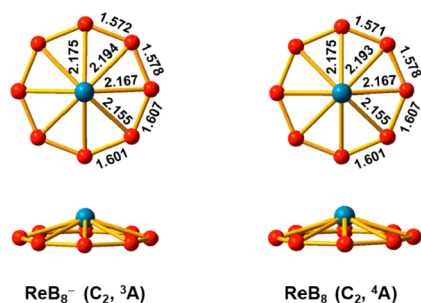**Figure 2.** Optimized structures of Re©B$_8^-$ and Re©B$_8$, along with their point groups and electronic states. Bond lengths are given in Å. The out-of-plane distortion of the Re atom is shown in a different perspective.
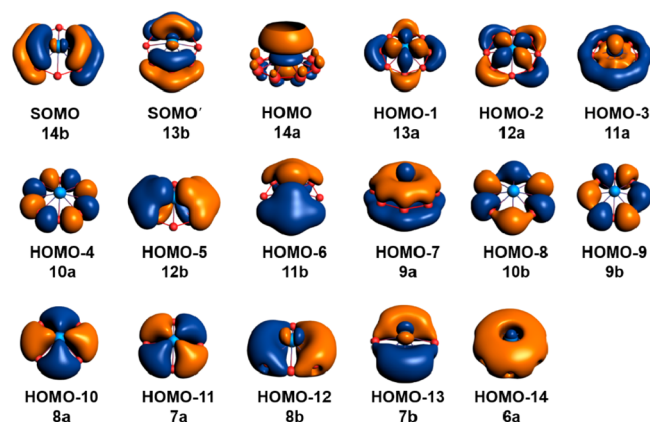

Figure 3. Valence molecular orbitals of Re©B$_8^-$ (C_2, ^{3}A) at the PBE0/TZP level.

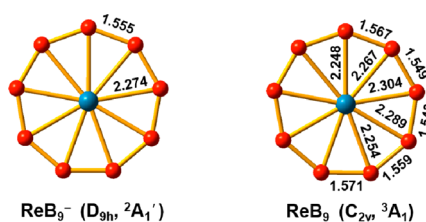**Figure 4.** Optimized structures of Re©B$_9^-$ and Re©B$_9$, along with their point groups and electronic states. Bond lengths are given in Å.

Re©B$_8^-$ structure are already longer than those in the perfectly planar borometallic molecular wheels, confirming the fact that the B$_8$ ring is too small to fit the Re atom.
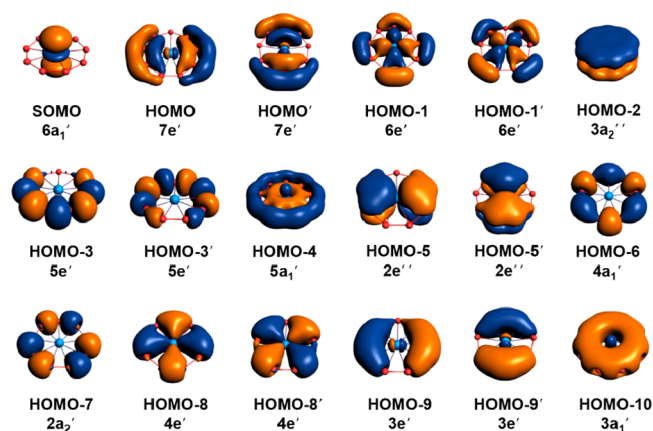

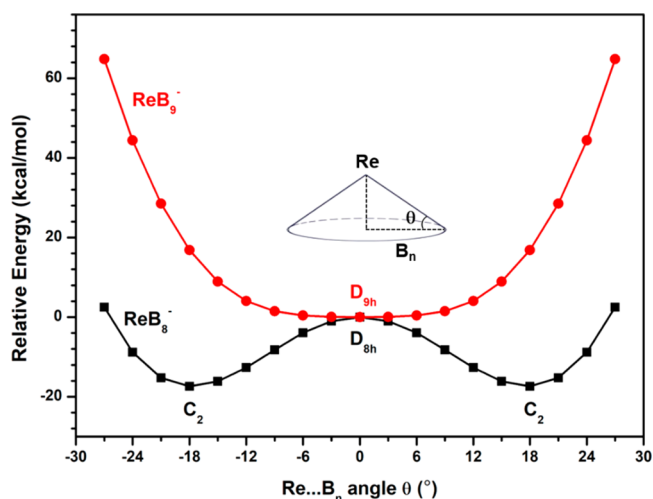**Figure 5.** Valence molecular orbitals of Re©B$_9^-$ (D_{9h}, ^{2}A$_1'$) at the PBE0/TZP level.

Figure 6. Relative GGA-PBE energies for Re©B$_8^-$ and Re©B$_9^-$ as functions of the Re···B$_n$ angle θ as defined in the inset. For each complex, the energy at $\theta = 0°$ is chosen to be zero.

The LT energy curve for Re©B$_9^-$ clearly shows that the D_{9h} structure is the true global minimum, suggesting that this complex fulfills both the electronic and geometrical design principles for the borometallic boron wheels.[21] It is interesting to note that the potential energy curve for the out-of-plane motion for Re©B$_9^-$ is quite flat near the equilibrium point, indicating a very low frequency out-of-plane bending vibrational motion by the Re atom.

5. DISCUSSION

5.1. Comparison between Experiment and Theory.

To validate the global-minimum C_2 structure for Re©B$_8^-$ and the D_{9h} structure for Re©B$_9^-$, we calculated their VDEs, as compared with the experimental data in Figure 1 and Tables 1 and 2, respectively, at the TD-SAOP/TZP level. The VDE$_1$ and ADE values for the C_2 Re©B$_8^-$ and D_{9h} Re©B$_9^-$ structures were computed at different levels of theory, as summarized in Table S2. The different levels of theory in general gave similar VDE$_1$ and ADE values, all in reasonable agreement with the experimental data. The DLPNO−CCSD(T)/Def2-TZVPP values were used to compute the higher VDEs in the TD-SAOP/TZP calculations given in Tables 1 and 2. The computed VDE$_1$ and ADE values are quite close to each other, consistent with the relatively small geometry changes between the ground states of the anion and neutral in each case, as shown in Figures 2 and 4. However, the experimentally estimated ADEs for both systems are significantly smaller than the corresponding VDE$_1$ values. This is probably due to the experimental difficulty of measuring the ADEs accurately as a result of the low spectral resolution and possible hot bands, which would give rise to large uncertainties in the estimation of the ADEs.

5.1.1. Re©B$_8^-$.

The computed VDE$_1$/ADE for the C_2 Re©B$_8^-$ global minimum were 3.79eV/3.75 eV at the DLPNO−CCSD(T)/Def2-TZVP level (Table S2), compared with the experimental data of 3.67eV/3.40 eV. As mentioned above, the ground state of the neutral is a quartet spin state, corresponding to the removal of an electron from the doubly occupied 14a orbital of mainly Re 5d$_{z^2}$ character (Figure 3). Detachment from the 14a orbital also gives rise to a final doublet state with a calculated VDE of 4.02 eV, in good agreement with band A at 3.97 eV (Figure 1a and Table 1). Detachments from the singly occupied 14b and 13b orbitals yield calculated VDEs of 5.02 and 5.15 eV, respectively, corresponding to the broad band C. Detachment transitions from the 13a and 12a orbitals give rise to four closely spaced detachment channels with calculated VDEs ranging from 5.41 to 5.63 eV. These transitions are consistent with the congested spectral feature around band D at ∼5.8 eV. Detachment from the 11a orbital yields two detachment channels with calculated VDEs of 6.32 eV for the quartet final state and 6.48 eV for the doublet final state, in agreement with band E at the high-binding-energy side. Theoretically, there is a large energy gap between the second (at 4.02 eV) and third (at 5.02 eV) detachment channels (Figure 1a and Table 1). However, a weak feature (B) is observed experimentally at 4.41 eV, which cannot be assigned to any of the computed single-electron detachment channels. This feature is likely derived from multielectron transitions due to strong electron correlation effects, which have been observed distinctly in the PES of B$_3^-$ previously.[67] Overall, the calculated VDEs of the C_2 Re©B$_8^-$ global minimum are in reasonable agreement with the experimental data, except for the weak band B.

5.1.2. Re©B$_9^-$.

The VDE$_1$/ADE calculated for the D_{9h} Re©B$_9^-$ molecular wheel are 4.04 eV/3.99 eV at the DLPNO−CCSD(T)/Def2-TZVPP level, in good agreement with the experimental data from band X of 4.02 eV/3.82 eV. As mentioned above, the first detachment channel is from the fully occupied 7e′ MO (Figure 5), resulting in a triplet spin state for neutral Re©B$_9$ (Figure 3). Detachment from the 7e′ orbital also produces a singlet final state with a calculated VDE

of 4.18 eV, which agrees well with band A at 4.34 eV. Detachments from the fully occupied 6e′ orbital yield two channels with calculated VDEs of 4.78 eV for the triplet final state and 4.98 eV for the singlet final state, which are in excellent agreement with band B at 4.63 eV and band C at 4.94 eV, respectively. Detachment from the 6a$_1'$ SOMO yields a calculated VDE of 5.25 eV, which likely corresponds to the unresolved feature on the higher-binding-energy side of the broad band C. Detachment transitions from the doubly occupied 3a$_2''$ orbital lead to triplet and singlet final states with calculated VDEs of 5.57 and 5.62 eV, respectively. These transitions are in good agreement with band D at 5.50 eV. Detachment channels from the 2e″, 5e′, and 5a$_1'$ orbitals result in three computed VDEs of 6.06, 6.32, and 6.43 eV, respectively, consistent with the broad band E at around 6.1 eV. The second detachment channels from these three MOs give rise to VDEs beyond the current spectral range. Overall, the calculated VDEs for the D_{9h} global minimum for Re©B$_9^-$ are in good agreement with the experimental data.

5.2. Chemical Bonding Analyses.

The perfect D_{9h} structure of Re©B$_9^-$ suggests that it fulfills both the electronic and geometrical design principles for borometallic molecular wheels. The MOs shown in Figure 5 indicate a single nonbonding 5d$_{z^2}$ electron, implying that six valence electrons of Re are involved in the delocalized bonding with the B$_9$ ring. On the other hand, the MOs of C_2 Re©B$_8^-$ (Figure 3) show a pair of electrons in the 5d$_{z^2}$ MO (14a), suggesting that five valence electrons of Re participate in bonding with the B$_8$ ring. To better understand the chemical bonding in the C_2 Re©B$_8^-$ and D_{9h} Re©B$_9^-$ molecular wheels and the differences between the two species, we performed AdNDP analyses, as shown in Figures 7 and 8, respectively.

The AdNDP results for C_2 Re©B$_8^-$ (Figure 7) reveal three 5d lone pairs (5d$_{z^2}$, 5d$_{xy}$, 5d$_{x^2-y^2}$) and eight 2c−2e B−B σ

1c-2e Re 5d$_{z^2}$
ON = 2.00 |e|

2 × 1c-2e Re 5d$_{xy}$/$_{x^2-y^2}$
ON = 1.73 |e|

8 × 2c-2e B-B σ bonds
ON = 1.95 |e|

2 × 9c-1e σ bonds
ON = 0.99 |e|

9c-2e σ bond
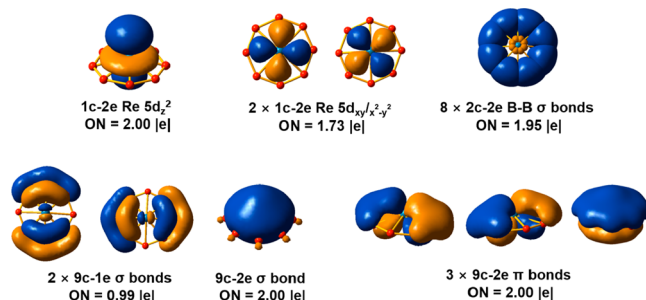ON = 2.00 |e|

3 × 9c-2e π bonds
ON = 2.00 |e|

Figure 7. AdNDP analyses of Re©B$_8^-$ (C_2, ^{3}A) at the PBE0/VTZ level.

bonds. There are also two sets of completely delocalized σ and π bonds. The three 9c−2e π bonds fulfill the $4N + 2$ Hückel rule for aromaticity. The three delocalized σ bonds include a 9c−2e bond and two 9c−1e bonds, which result in the triplet ground state for Re©B$_8^-$. Hence, the delocalized σ bonds fulfill the modified Hückel rule ($4N$) for aromaticity for molecules with triplet states.[68] Therefore, C_2 Re©B$_8^-$ can still be considered to be doubly aromatic. It is seen that the AdNDP analyses give a better picture about the chemical bonding in Re©B$_8^-$ than the MOs. Given the availability of 5d electrons on the Re center, an interesting question is why are no more electrons transferred to the delocalized σ bonds? The answer can be glimpsed from the MOs shown in Figure 3. The two 9c−1e σ bonds mainly come from the two SOMOs (13b and

14a). Because the B_8 ring is too small to fit the Re atom, it is squeezed out of plane, making the two delocalized σ MOs energetically less favorable. Therefore, the $5d_{xy}$ and $5d_{x^2-y^2}$ electrons largely remain localized on the Re center. The 1.73 |e| occupation numbers (ONs) for the $5d_{xy}$ and $5d_{x^2-y^2}$ lone pairs (Figure 7) suggest that they participate in delocalized bonding to a small degree. Hence, even though the electronic design principle can be fulfilled for the Re©B_8^- molecular wheel, the geometrical design principle is not met, resulting in its out-of-plane distortion and its triplet electronic state.

The AdNDP analyses for D_{9h} Re©B_9^- (Figure 8) reveal five 5d electrons on Re (a single electron in $5d_{z^2}$ and two $5d_{xy}/$
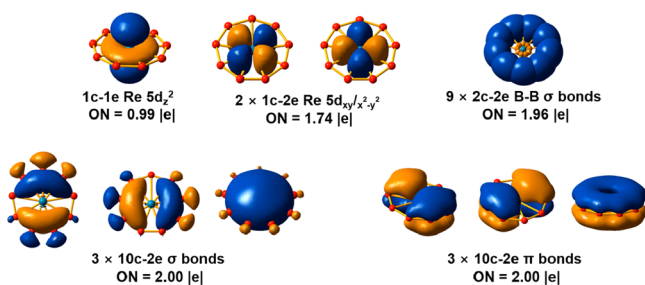

Figure 8. AdNDP analyses of ReB_9^- (D_{9h}, $^2A_1'$) at the PBE0/VTZ level.

$5d_{x^2-y^2}$ lone pairs) and nine 2c−2e B−B σ bonds in addition to two sets of three completely delocalized σ and π bonds. The latter suggest that Re©B_9^- is doubly aromatic and fulfills both the electronic and geometrical design principles to form the perfectly planar borometallic molecular wheels. Even though the ONs of the $5d_{xy}$ and $5d_{x^2-y^2}$ lone pairs (1.74 |e| in Figure 8) are smaller than 2, indicating a small degree of covalent interactions with the B_9 ring, they certainly cannot be counted as part of the delocalized σ system. Hence, the Re©B_9^- molecular wheel obeys the $n + x + k = 12$ electronic design principle for late transition metals (Fe, Co, Ru, Rh, Ir),[32−34] rather than the $n + x + k = 16$ electronic design principle for early transition metals (Nb and Ta).[35−38] On the basis of the bonding analyses of B_8 and B_9 using the local coordinate systems, the formal oxidation states of Re in the Re©B_8^- and Re©B_9^- molecular wheels are assigned as +I and +II, respectively, which are consistent with the electrons located on the 5d orbitals from the semilocalized AdNDP results. The Re atom assumes rather low oxidation states in these systems because of the low electronegativity of boron, as has been shown recently in other binary metal−boron clusters.[69,70] The current work demonstrates that borometallic molecular wheels ($M©B_n^q$) can be formed for all transition metals from group VB to group VIIIB.

6. CONCLUSIONS

We have reported a joint photoelectron spectroscopy and quantum-chemical study of two rhenium-doped boron clusters, Re©B_8^- and Re©B_9^-. Global-minimum searches found that the Re©B_8^- cluster has a triplet ground state with a pseudo-C_{8v} structure (C_2, ^3A), whereas the Re©B_9^- cluster has a doublet ground state with a perfect Re-centered D_{9h} structure ($^2A_1'$). The calculated vertical detachment energies were compared with the experimental data to verify the global minima. Chemical bonding analyses revealed that both Re©B_8^- and Re©B_9^- are doubly aromatic with three delocalized σ and π bonds, with Re©B_8^- containing two one-electron delocalized σ

bonds obeying the Hückel rule for triplet states. The Re atom adopts unusual +I and +II oxidation states in Re©B_8^- and Re©B_9^-, respectively. The D_{9h} Re©B_9^- cluster is found to fulfill both the electronic and geometrical design principles similar to the late-transition-metal-doped molecular wheels, while the B_8 ring is too small to fit the Re atom, leading to the distortion to C_2 symmetry even though it obeys the electronic design principle. The Re©B_8^- and Re©B_9^- clusters are additions to the family of transition-metal-centered borometallic molecular wheels ($M@B_n^q$). These highly stable and symmetric molecular wheels may be viable for bulk syntheses with appropriate ligands to coordinate to the metal centers.

■ ASSOCIATED CONTENT

Ⓢ Supporting Information

The Supporting Information is available free of charge on the ACS Publications website at DOI: 10.1021/acs.jpca.9b03942.

> Low-lying isomers of ReB_8^- and ReB_9^- within 50 kcal/mol of the global minima; the coordinates of the global minima of Re©B_8^-, Re©B_9^-, and their neutrals; and the first VDEs and ADEs of Re©B_8^- and Re©B_9^- calculated at different levels of theory (PDF)

■ AUTHOR INFORMATION

Corresponding Authors
*E-mail: junli@tsinghua.edu.cn (J.L.).
*E-mail: lai-sheng_wang@brown.edu (L.S.W.).

ORCID Ⓞ
Jun Li: 0000-0002-8456-3980
Lai-Sheng Wang: 0000-0003-1816-5738

Present Address
⊥H.B.: On leave from the Key Laboratory of Coal Science and Technology of Ministry of Education and Shanxi Province, Taiyuan University of Technology, Taiyuan, Shanxi 030024, China.

Author Contributions
∥T.-T.C. and W.-L.L. contributed equally to this work.

Notes
The authors declare no competing financial interest.

■ REFERENCES

(1) Albert, B.; Hillebrecht, H. Boron: Elementary Challenge for Experimenters and Theoreticians. *Angew. Chem., Int. Ed.* **2009**, *48*, 8640−8668.

(2) Oganov, A. R.; Chen, J.; Gatti, C.; Ma, Y.; Ma, Y.; Glass, C. W.; Liu, Z.; Yu, T.; Kurakevych, O. O.; Solozhenko, V. L. Ionic High-Pressure Form of Elemental Boron. *Nature* **2009**, *457*, 863−867.

(3) Alexandrova, A. N.; Boldyrev, A. I.; Zhai, H. J.; Wang, L. S. All-Boron Aromatic Clusters as Potential New Inorganic Ligands and

Building Blocks in Chemistry. *Coord. Chem. Rev.* **2006**, *250*, 2811−2866.

(4) Sergeeva, A. P.; Popov, I. A.; Piazza, Z. A.; Li, W. L.; Romanescu, C.; Wang, L. S.; Boldyrev, A. I. Understanding Boron through Size-Selected Clusters: Structure, Chemical Bonding, and Fluxionality. *Acc. Chem. Res.* **2014**, *47*, 1349−1358.

(5) Wang, L. S. Photoelectron Spectroscopy of Size-Selected Boron Clusters: From Planar Structures to Borophenes and Borospherenes. *Int. Rev. Phys. Chem.* **2016**, *35*, 69−142.

(6) Li, W. L.; Chen, X.; Jian, T.; Chen, T. T.; Li, J.; Wang, L. S. From Planar Boron Clusters to Borophenes and Metalloborophenes. *Nat. Rev. Chem.* **2017**, *1*, 0071.

(7) Kiran, B.; Bulusu, S.; Zhai, H. J.; Yoo, S.; Zeng, X. C.; Wang, L. S. Planar-to-Tubular Structural Transition in Boron Clusters: B_{20} as the Embryo of Single-Walled Boron Nanotubes. *Proc. Natl. Acad. Sci. U. S. A.* **2005**, *102*, 961−964.

(8) Oger, E.; Crawford, N. R.; Kelting, R.; Weis, P.; Kappes, M. M.; Ahlrichs, R. Boron Cluster Cations: Transition from Planar to Cylindrical Structures. *Angew. Chem., Int. Ed.* **2007**, *46*, 8503−8506.

(9) Piazza, Z. A.; Hu, H. S.; Li, W. L.; Zhao, Y. F.; Li, J.; Wang, L. S. Planar Hexagonal B_{36} as a Potential Basis for Extended Single-Atom Layer Boron Sheets. *Nat. Commun.* **2014**, *5*, 3113.

(10) Li, W. L.; Chen, Q.; Tian, W. J.; Bai, H.; Zhao, Y. F.; Hu, H. S.; Li, J.; Zhai, H. J.; Li, S. D.; Wang, L. S. The B_{35} Cluster with a Double-Hexagonal Vacancy: A New and More Flexible Structural Motif for Borophene. *J. Am. Chem. Soc.* **2014**, *136*, 12257−12260.

(11) Zhai, H. J.; Zhao, Y. F.; Li, W. L.; Chen, Q.; Bai, H.; Hu, H. S.; Piazza, Z. P.; Tian, W. J.; Lu, H. G.; Wu, Y. B.; et al. Observation of an All-Boron Fullerene. *Nat. Chem.* **2014**, *6*, 727−731.

(12) Chen, Q.; Li, W. L.; Zhao, Y. F.; Zhang, S. Y.; Hu, H. S.; Bai, H.; Li, H. R.; Tian, W. J.; Lu, H. G.; Zhai, H. J.; et al. Experimental and Theoretical Evidence of An Axially Chiral Borospherene. *ACS Nano* **2015**, *9*, 754−760.

(13) Nagamatsu, J.; Nakagawa, N.; Muranaka, T.; Zenitani, Y.; Akimitsu, J. Superconductivity at 39 K in Magnesium Diboride. *Nature* **2001**, *410*, 63−64.

(14) Chung, H.-Y.; Weinberger, M. B.; Levine, J. B.; Kavner, A.; Yang, J.-M.; Tolbert, S. H.; Kaner, R. B. Synthesis of Ultra-Incompressible Superhard Rhenium Diboride at Ambient Pressure. *Science* **2007**, *316*, 436−439.

(15) Scheifers, J. P.; Zhang, Y.; Fokwa, B. P. T. Boron: Enabling Exciting Metal-Rich Structures and Magnetic Properties. *Acc. Chem. Res.* **2017**, *50*, 2317−2325.

(16) Tian, F.; Ren, Z. High Thermal Conductivity in Boron Arsenide: From Prediction to Reality. *Angew. Chem., Int. Ed.* **2019**, *58*, 5824−5831.

(17) Jian, T.; Chen, X. N.; Li, S. D.; Boldyrev, A. I.; Li, J.; Wang, L. S. Probing the Structures and Bonding of Size-Selected Boron and Doped-Boron Clusters. *Chem. Soc. Rev.* **2019**, DOI: 10.1039/C9CS00233B.

(18) Robinson, P. J.; Zhang, X. X.; McQueen, T.; Bowen, K. H.; Alexandrova, A. N. SmB_6^- Cluster Anions: Covalency Involving f Orbitals. *J. Phys. Chem. A* **2017**, *121*, 1849−1854.

(19) Robinson, P. J.; Liu, G. X.; Ciborowski, S.; Martinez-Martinez, C.; Chamorro, J. R.; Zhang, X. X.; McQueen, T.; Bowen, K. H.; Alexandrova, A. N. Mystery of Three Borides: Differential Metal-Boron Bonding Governing Superhard Structures. *Chem. Mater.* **2017**, *29*, 9892−9896.

(20) Mason, J. L.; Harb, H.; Huizenga, C. D.; Ewigleben, J. C.; Topolski, J. E.; Hratchian, H. P.; Jarrold, C. C. Electronic and Molecular Structures of CeB_6 Monomer. *J. Phys. Chem. A* **2019**, *123*, 2040−2048.

(21) Romanescu, C.; Galeev, T. R.; Li, W. L.; Boldyrev, A. I.; Wang, L. S. Transition-Metal-Centered Monocyclic Boron Wheel Clusters ($M©B_n$): A New Class of Aromatic Borometallic Compounds. *Acc. Chem. Res.* **2013**, *46*, 350−358.

(22) Popov, I. A.; Li, W. L.; Piazza, Z. A.; Boldyrev, A. I.; Wang, L. S. Complexes between Planar Boron Clusters and Transition Metals: A

(23) Photoelectron Spectroscopy and Ab Initio Study of CoB_{12}^- and RhB_{12}^-. *J. Phys. Chem. A* **2014**, *118*, 8098−8105.

(23) Chen, T.-T.; Li, W.-L.; Jian, T.; Chen, X.; Li, J.; Wang, L. S. PrB_7^-: A Praseodymium-Doped Boron Cluster with a Pr^{II} Center Coordinated by a Doubly Aromatic Planar η^7-B_7^{3-} Ligand. *Angew. Chem., Int. Ed.* **2017**, *56*, 6916−6920.

(24) Li, W. L.; Jian, T.; Chen, X.; Chen, T. T.; Lopez, G. V.; Li, J.; Wang, L. S. The Planar CoB_{18}^- Cluster as a Motif for Metallo-Borophenes. *Angew. Chem., Int. Ed.* **2016**, *55*, 7358−7363.

(25) Jian, T.; Li, W. L.; Chen, X.; Chen, T. T.; Lopez, G. V.; Li, J.; Wang, L. S. Competition between Drum and Quasi-Planar Structures in RhB_{18}^-: Motifs for Metallo-Boronanotubes and Metallo-Borophenes. *Chem. Sci.* **2016**, *7*, 7020−7027.

(26) Popov, I. A.; Jian, T.; Lopez, G. V.; Boldyrev, A. I.; Wang, L. S. Cobalt-Centred Boron Molecular Drums with the Highest Coordination Number in the CoB_{16}^- Cluster. *Nat. Commun.* **2015**, *6*, 8654.

(27) Jian, T.; Li, W. L.; Popov, I. A.; Lopez, G. V.; Chen, X.; Boldyrev, A. I.; Li, J.; Wang, L. S. Manganese-Centered Tubular Boron Cluster−MnB_{16}^-: A New Class of Transition-Metal Molecules. *J. Chem. Phys.* **2016**, *144*, 154310.

(28) Li, W. L.; Jian, T.; Chen, X.; Li, H. R.; Chen, T. T.; Luo, X. M.; Li, S. D.; Li, J.; Wang, L. S. Observation of a Metal-Centered B_2-Ta@B_{18}^- Tubular Molecular Rotor and a Perfect Ta@B_{20}^- Boron Drum with the Record Coordination Number of Twenty. *Chem. Commun.* **2017**, *53*, 1587−1590.

(29) Li, W. L.; Xie, L.; Jian, T.; Romanescu, C.; Huang, X.; Wang, L. S. Hexagonal Bipyramidal $[Ta_2B_6]^{-/0}$ Clusters: B_6 Rings as Structural Motifs. *Angew. Chem., Int. Ed.* **2014**, *53*, 1288−1292.

(30) Li, W. L.; Chen, T. T.; Xing, D. H.; Chen, X.; Li, J.; Wang, L. S. Observation of Highly Stable and Symmetric Lanthanide Octa-Boron Inverse Sandwich Complexes. *Proc. Natl. Acad. Sci. U. S. A.* **2018**, *115*, E6972−E6977.

(31) Chen, T. T.; Li, W. L.; Li, J.; Wang, L. S. $[La (\eta^x$-$B_x)$ La]$^-$ (x = 7−9): A New Class of Inverse Sandwich Complexes. *Chem. Sci.* **2019**, *10*, 2534−2542.

(32) Romanescu, C.; Galeev, T. R.; Li, W. L.; Boldyrev, A. I.; Wang, L. S. Aromatic Metal-Centered Monocyclic Boron Rings: $Co©B_8^-$ and $Ru©B_9^-$. *Angew. Chem., Int. Ed.* **2011**, *50*, 9334−9337.

(33) Li, W. L.; Romanescu, C.; Galeev, T. R.; Piazza, Z. A.; Boldyrev, A. I.; Wang, L. S. Transition-Metal-Centered Nine-Membered Boron Rings: $M©B_9$ and $M©B_9^-$ (M = Rh, Ir). *J. Am. Chem. Soc.* **2012**, *134*, 165−168.

(34) Romanescu, C.; Galeev, T. R.; Sergeeva, A. P.; Li, W. L.; Wang, L. S.; Boldyrev, A. I. Experimental and Computational Evidence of Ccta-and Nona-Coordinated Planar Iron-Doped Boron Clusters: $Fe©B_8^-$ and $Fe©B_9^-$. *J. Organomet. Chem.* **2012**, *721*, 148−154.

(35) Galeev, T. R.; Romanescu, C.; Li, W. L.; Wang, L. S.; Boldyrev, A. I. Observation of the Highest Coordination Number in Planar Species: Decacoordinated $Ta©B_{10}^-$ and $Nb©B_{10}^-$ Anions. *Angew. Chem., Int. Ed.* **2012**, *51*, 2101−2105.

(36) Li, W. L.; Romanescu, C.; Piazza, Z. A.; Wang, L. S. Geometrical Requirements for Transition-Metal-Centered Aromatic Boron Wheels: The Case of VB_{10}^-. *Phys. Chem. Chem. Phys.* **2012**, *14*, 13663−13669.

(37) Li, W. L.; Ivanov, A. S.; Federič, J.; Romanescu, C.; Černušák, I.; Boldyrev, A. I.; Wang, L. S. On the Way to the Highest Coordination Number in the Planar Metal-Centred Aromatic $Ta©B_{10}^-$ Cluster: Evolution of the Structures of TaB_n^- (n = 3−8). *J. Chem. Phys.* **2013**, *139*, 104312.

(38) Romanescu, C.; Galeev, T. R.; Li, W. L.; Boldyrev, A. I.; Wang, L. S. Geometric and Electronic Factors in the Rational Design of Transition-Metal-Centered Boron Molecular Wheels. *J. Chem. Phys.* **2013**, *138*, 134315.

(39) Heine, T.; Merino, G. What IS the Maximum Coordination Number in a Planar Structure? *Angew. Chem., Int. Ed.* **2012**, *51*, 4275−4276.

(40) Ito, K.; Pu, Z.; Li, Q. S.; Schleyer, P. v. R. Cyclic Boron Clusters Enclosing Planar Hypercoordinate Cobalt, Iron, and Nickel. *Inorg. Chem.* **2008**, *47*, 10906−10910.

(41) Pu, Z. F.; Ito, K.; Schleyer, P. v. R.; Li, Q. S. Planar Hepta-, Ota-, Nona-, and Decacoordinate First Row d-Block Metals Enclosed by Boron Rings. *Inorg. Chem.* **2009**, *48*, 10679−10686.

(42) Zhao, R. N.; Yuan, Y. H.; Han, J. G. Transition Metal Mo-Doped Boron Clusters: A Computational Investigation. *J. Theor. Comput. Chem.* **2014**, *13*, 1450036.

(43) Yang, L. M.; Ganz, E.; Chen, Z. F.; Wang, Z. X.; Schleyer, P. V. Four Decades of the Chemistry of Planar Hypercoordinate Compounds. *Angew. Chem., Int. Ed.* **2015**, *54*, 9468−9501.

(44) Zhao, R. N.; Yuan, Y. H.; Han, J. G. Geometric and Electronic Properties of Transition Metal Hafnium-Doped Boron Clusters: A Computational Investigation. *Polycyclic Aromat. Compd.* **2016**, *36*, 252−272.

(45) Li, P. F.; Mei, T. T.; Lv, L. X.; Lu, C.; Wang, W. H.; Bao, G.; Gutsev, G. L. Structure and Electronic Properties of Neutral and Negatively Charged RhB_n Clusters ($n = 3-10$): A Density Functional Theory Study. *J. Phys. Chem. A* **2017**, *121*, 6510−6516.

(46) Pan, S.; Kar, S.; Saha, R.; Osorio, E.; Zarate, X.; Zhao, L. L.; Merino, G.; Chattaraj, P. K. Boron Nanowheels with Axles Containing Noble Gas Atoms: Viable Noble Gas Bound $M©B_{10}^-$ Clusters (M = Nb, Ta). *Chem. - Eur. J.* **2018**, *24*, 3590−3598.

(47) Li, P.; Du, X.; Wang, J. J.; Lu, C.; Chen, H. Probing the Structural Evolution and Stabilities of Medium-Sized $MoB_n^{0/-}$ Clusters. *J. Phys. Chem. C* **2018**, *122*, 20000−20005.

(48) Wang, L. S.; Cheng, H. S.; Fan, J. Photoelectron Spectroscopy of Size-Selected Transition Metal Clusters: Fe_n^-, n = 3−24. *J. Chem. Phys.* **1995**, *102*, 9480−9493.

(49) Zhao, Y.; Chen, X.; Li, J. TGMin: A Global-Minimum Structure Search Program Based on a Constrained Basin-Hopping Algorithm. *Nano Res.* **2017**, *10*, 3407−3420.

(50) Chen, X.; Zhao, Y. F.; Wang, L. S.; Li, J. Recent Progresses of Global Minimum Searches of Nanoclusters with a Constrained Basin-Hopping Algorithm in the TGMin Program. *Comput. Theor. Chem.* **2017**, *1107*, 57−65.

(51) Chen, X.; Zhao, Y. F.; Zhang, Y. Y.; Li, J. TGMin: An Efficient Global Minimum Searching Program for Free and Surface-Supported Clusters. *J. Comput. Chem.* **2018**, *40*, 1105−1112.

(52) Perdew, J. P.; Burke, K.; Ernzerhof, M. Generalized Gradient Approximation Made Simple. *Phys. Rev. Lett.* **1996**, *77*, 3865−3868.

(53) van Lenthe, E.; Baerends, E. J. Optimized Slater-type Basis Sets for the Elements 1−118. *J. Comput. Chem.* **2003**, *24*, 1142−1156.

(54) *ADF*, version 2017.114; SCM: Amsterdam, 2017; http://www.scm.com.

(55) van Lenthe, E.; Baerends, E. J.; Snijders, J. G. Relativistic Regular Two-Component Hamiltonians. *J. Chem. Phys.* **1993**, *99*, 4597−4610.

(56) Adamo, C.; Barone, V. Toward Reliable Density Functional Methods without Adjustable Parameters: The PBE0 Model. *J. Chem. Phys.* **1999**, *110*, 6158−6170.

(57) Li, J.; Li, X.; Zhai, H. J.; Wang, L. S. Au_{20}: A Tetrahedral Cluster. *Science* **2003**, *299*, 864−867.

(58) Gritsenko, O. V.; Schipper, P. R. T.; Baerends, E. J. Approximation of the Exchange−Correlation Kohn−Sham Potential with a Statistical Average of Different Orbital Model Potentials. *Chem. Phys. Lett.* **1999**, *302*, 199−207.

(59) Neese, F.; Wennmohs, F.; Hansen, A. Efficient and Accurate Local Approximations to Coupled-Electron Pair Approaches: An Attempt to Revive the Pair Natural Orbital Method. *J. Chem. Phys.* **2009**, *130*, 114108.

(60) Neese, F.; Hansen, A.; Liakos, D. G. Efficient and Accurate Approximations to the Local Coupled Cluster Singles Doubles Method Using a Truncated Pair Natural Orbital Basis. *J. Chem. Phys.* **2009**, *131*, 064103.

(61) Stoychev, G. L.; Auer, A. A.; Neese, F. Automatic Generation of Auxiliary Basis Sets. *J. Chem. Theory Comput.* **2017**, *13*, 554−562.

(62) Weigend, F.; Ahlrichs, R. Balanced Basis Sets of Split Valence, Triple Zeta Valence and Quadruple Zeta Valence Quality for H to Rn: Design and Assessment of Accuracy. *Phys. Chem. Chem. Phys.* **2005**, *7*, 3297−3305.

(63) Andrae, D.; Häußermann, U.; Dolg, M.; Stoll, H.; Preuß, H. Energy-Adjusted Ab Initio Pseudopotentials for the Second and Third Row Transition Elements. *Theor. Chim. Acta* **1990**, *77*, 123−141.

(64) Figgen, D.; Peterson, K. A.; Dolg, M.; Stoll, H. Energy-Consistent Pseudopotentials and Correlation Consistent Basis Sets for the 5d Elements Hf−Pt. *J. Chem. Phys.* **2009**, *130*, 164108.

(65) Dunning, T. H., Jr Gaussian Basis Sets for Use in Correlated Molecular Calculations. I. The Atoms Boron through Neon and Hydrogen. *J. Chem. Phys.* **1989**, *90*, 1007−1023.

(66) Zubarev, D. Y.; Boldyrev, A. I. Developing Paradigms of Chemical Bonding: Adaptive Natural Density Partitioning. *Phys. Chem. Chem. Phys.* **2008**, *10*, 5207−5217.

(67) Zhai, H. J.; Wang, L. S.; Alexandrova, A. N.; Boldyrev, A. I.; Zakrzewski, V. G. A Photoelectron Spectroscopy and *Ab Initio* Study of B_3^- and B_4^- Anions and Their Neutrals. *J. Phys. Chem. A* **2003**, *107*, 9319−9328.

(68) Baird, N. C. Quantum Organic Photochemistry. II. Resonance and Aromaticity in the Lowest $^3\pi\pi*$ State of Cyclic Hydrocarbons. *J. Am. Chem. Soc.* **1972**, *94*, 4941−4948.

(69) Chen, X.; Chen, T. T.; Li, W. L.; Lu, J. B.; Zhao, L. J.; Jian, T.; Hu, H. S.; Wang, L. S.; Li, J. Lanthanides with Unusually Low Oxidation States in the PrB_3^- and PrB_4^- Boride Clusters. *Inorg. Chem.* **2019**, *58*, 411−418.

(70) Li, W. L.; Chen, T. T.; Jiang, Z. Y.; Chen, W. J.; Hu, H. S.; Wang, L. S.; Li, J. Probing the Electronic Structure of the CoB_{16}^- Drum Complex: Unusual Oxidation State of Co(−I). *Chin. J. Chem. Phys.* **2019**, *32*, 241−247.